Acta Crystallographica Section A
Foundations and Advances
ISSN 2053-2733

Received 10 October 2013
Accepted 6 December 2013

Magnetic pair distribution function analysis of local magnetic correlations

Benjamin A. Frandsen,[a] Xiaohao Yang[b] and Simon J. L. Billinge[b,c]*

[a]Department of Physics, Columbia University, New York, NY 10027, USA, [b]Department of Applied Physics and Applied Mathematics, Columbia University, New York, NY 10027, USA, and [c]Condensed Matter Physics and Materials Science Department, Brookhaven National Laboratory, Upton, NY 11973, USA. Correspondence e-mail: sb2896@columbia.edu

The analytical form of the magnetic pair distribution function (mPDF) is derived for the first time by computing the Fourier transform of the neutron scattering cross section from an arbitrary collection of magnetic moments. Similar to the atomic pair distribution function applied to the study of atomic structure, the mPDF reveals both short-range and long-range magnetic correlations directly in real space. This function is experimentally accessible and yields magnetic correlations even when they are only short-range ordered. The mPDF is evaluated for various example cases to build an intuitive understanding of how different patterns of magnetic correlations will appear in the mPDF.

1. Introduction

Emergent phenomena in complex materials represent one of the most exciting and challenging fields of research in modern condensed matter physics (Dagotto, 2005). Exotic behavior such as high-temperature superconductivity (Dagotto, 1994; Orenstein & Millis, 2000; Lee *et al.*, 2006; Basov & Chubukov, 2011), colossal magnetoresistance (Millis, 1998; Dagotto *et al.*, 2001; Dagotto, 2005), multiferroism (Eerenstein *et al.*, 2006; Cheong & Mostovoy, 2007) and relaxor ferroelectricity (Cross, 1987; Bokov & Ye, 2006) exemplify the strong overlap of both fundamental and applied interest in these types of systems.

As the body of research into these materials grows, it is becoming increasingly evident that short-range structural correlations and phase fluctuations on the nanoscale underlie many of their fascinating properties (Imada *et al.*, 1998; Uehara *et al.*, 1999; Fath *et al.*, 1999; Chuang *et al.*, 2001; Dagotto *et al.*, 2003; Billinge & Kanatzidis, 2004; Dagotto, 2005; Billinge & Levin, 2007). A crucial first step toward understanding the behavior of these systems is to accurately determine the detailed structure of their lattice, charge, orbital and spin degrees of freedom (Millis, 1998). Unfortunately, the very characteristic that makes these systems so interesting – the presence of nanoscale correlations and fluctuations – makes many conventional methods of structure determination, X-ray and neutron diffraction in particular, unreliable at best and completely ineffectual at worst (Billinge & Levin, 2007). Traditional diffraction techniques are sensitive only to the average long-range structure of a material, and are therefore poorly suited to investigating the local short-range order of interest in complex materials.

Over the past two decades, significant progress has been made through the development of total scattering techniques to determine local atomic structure (Egami & Billinge, 2013; Tucker *et al.*, 2001, 2007; Proffen *et al.*, 2003; Juhás *et al.*, 2006; Young & Goodwin, 2011). Total scattering refers to the detection and analysis of both Bragg scattering, corresponding to long-range order, and diffuse scattering, arising from short-range correlations deviating from the average structure. Pair distribution function (PDF) analysis (Egami & Billinge, 2013) has proven to be an especially effective tool for investigating complex materials, and it is also quickly becoming indispensable in the burgeoning fields of nanoscience and nanotechnology (Egami & Billinge, 2013; Billinge & Levin, 2007). PDF analysis involves Fourier transforming the scattered X-ray or neutron intensity from momentum space into real space, yielding the real-space pair correlation function.

There are numerous benefits to this type of real-space analysis. Most notably, short-range order, which gives rise to diffuse features in momentum space that are not ideal for fitting purposes, manifests itself through relatively sharp features in the real-space correlation function, making quantitative fits much more feasible (Egami & Billinge, 2013). Real-space signals are also often easier to interpret intuitively, leading to deeper understanding and more effective model proposal. For these reasons, PDF analysis has proven itself to be a powerful probe of short-range atomic correlations in complex materials. We hope that the mPDF (magnetic pair distribution function) will, likewise, yield useful insights into magnetic correlations in materials.

Along with local atomic structure, local magnetic structure also plays a critical role in a host of condensed matter phenomena, including such well known examples as spin–stripe correlations in cuprate superconductors (Tranquada *et al.*, 1996, 1997), spin fluctuations in frustrated magnetic systems such as the quantum spin liquid herbertsmithite (Han *et al.*, 2012) and spin order in diluted magnetic semiconductors (Furdyna, 1988; Ohno, 1998; Zhao *et al.*, 2013). Neutron

scattering has long been one of the foremost experimental techniques used to investigate magnetic structure. However, the short-range nature of the magnetic correlations of interest render conventional neutron diffraction less effective. Reverse Monte Carlo techniques have been used successfully by iteratively fitting randomly generated structural models in momentum space (Keen & McGreevy, 1991; Paddison & Goodwin, 2012), indicating that diffuse magnetic scattering can be rich in information. However, as in the case of atomic structure, there may be distinct advantages to performing the analysis in real space after Fourier transforming the scattered intensity, and we explore that here.

Up until now, real-space investigations of magnetic correlations have been infrequent and less than optimally effective. Wu *et al.*, for instance, transformed the magnetic scattering intensity into real space and made qualitative inferences from it, but did not attempt to extract any quantitative information or derive a functional form of the real-space magnetic correlation function (Wu *et al.*, 1987). Blech and Averbach performed quantitative fits in real space by transforming the experimental signal from momentum space to real space, but the theoretical real-space signal was obtained by first calculating the momentum-space signal and then numerically transforming it into real space (Blech & Averbach, 1964).

A more direct approach is to compute analytically the Fourier transform of the magnetic scattering intensity to obtain the real-space correlation function, which we call the mPDF in analogy to the atomic PDF, and to fit this to the transformed real-space data. In the following, we will derive an expression for the mPDF and comment on its physical meaning and utility.

2. Derivation of the mPDF equations

We begin with the result first obtained by Blech & Averbach (1964) for the orientationally averaged magnetic scattering cross section of neutrons from a system of identical localized spins in the quasistatic approximation,

$$\frac{\mathrm{d}\sigma}{\mathrm{d}\Omega} = \frac{2}{3}N\,S(S+1)(\gamma r_0)^2 f^2 + (\gamma r_0)^2 f^2 \times \sum_{i\neq j}\left\{A_{ij}\frac{\sin\kappa r_{ij}}{\kappa r_{ij}} + B_{ij}\left[\frac{\sin\kappa r_{ij}}{(\kappa r_{ij})^3} - \frac{\cos\kappa r_{ij}}{(\kappa r_{ij})^2}\right]\right\}, \quad (1)$$

where the subscripts i and j refer to individual magnetic moments $\mathbf{S}_i$ and $\mathbf{S}_j$ separated by a distance r_{ij}, $A_{ij} = \langle S_i^y S_j^y\rangle$, $B_{ij} = 2\langle S_i^x S_j^x\rangle - \langle S_i^y S_j^y\rangle$, S is the spin quantum number in units of $\hbar$, $r_0 = (\mu_0/4\pi)(e^2/m_e)$ is the classical electron radius, $\gamma = 1.913$ is the neutron magnetic moment in units of nuclear magnetons, f is the magnetic form factor, N is the number of spins in the system and κ is the magnitude of the scattering vector, with the symbol chosen so as to avoid confusion with the magnetic scattering operator, conventionally denoted $\mathbf{Q}$. The angled brackets $\langle\cdots\rangle$ denote a quantum mechanical average. The first term results from self-scattering (*i.e.* $i = j$) and is equivalent to the scattering from a collection of completely randomly oriented spins. The coordinate system used to express A_{ij} and B_{ij} is locally defined for each spin pair through

$$\hat{\mathbf{x}} = \frac{\mathbf{r}_j - \mathbf{r}_i}{|\mathbf{r}_j - \mathbf{r}_i|} \text{ and } \hat{\mathbf{y}} = \frac{\mathbf{S}_i - \hat{\mathbf{x}}(\mathbf{S}_i\cdot\hat{\mathbf{x}})}{|\mathbf{S}_i - \hat{\mathbf{x}}(\mathbf{S}_i\cdot\hat{\mathbf{x}})|},$$

as shown in Fig. 1.

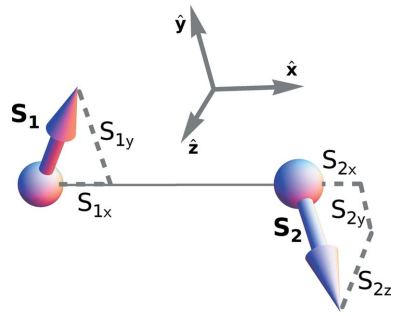

Figure 1
Local coordinate system used in equation (1).

We obtain the magnetic structure factor $S(\kappa)$ by dividing out the self-scattering contribution:

$$S(\kappa) = \frac{\mathrm{d}\sigma/\mathrm{d}\Omega}{\frac{2}{3}N\,S(S+1)(\gamma r_0)^2 f^2} = 1 + \frac{1}{N}\frac{3}{2S(S+1)} \times \sum_{i\neq j}\left\{A_{ij}\frac{\sin\kappa r_{ij}}{\kappa r_{ij}} + B_{ij}\left[\frac{\sin\kappa r_{ij}}{(\kappa r_{ij})^3} - \frac{\cos\kappa r_{ij}}{(\kappa r_{ij})^2}\right]\right\}. \quad (2)$$

Defining the reduced structure function as $F(\kappa) = \kappa[S(\kappa) - 1]$, we have

$$F(\kappa) = \frac{1}{N}\frac{3}{2S(S+1)} \times \sum_{i\neq j}\left[A_{ij}\frac{\sin\kappa r_{ij}}{r_{ij}} + B_{ij}\left(\frac{\sin\kappa r_{ij}}{\kappa^2 r_{ij}^3} - \frac{\cos\kappa r_{ij}}{\kappa r_{ij}^2}\right)\right]. \quad (3)$$

Expressing the scattered intensity in terms of this reduced structure function effectively removes the contributions from self-scattering. We now Fourier transform this quantity into real space:

$$f(r) = \frac{2}{\pi}\int_0^\infty \mathrm{d}\kappa F(\kappa)\sin\kappa r \quad (4)$$

$$= \frac{1}{N}\frac{3}{2S(S+1)}\sum_{i\neq j}\left\{\frac{A_{ij}}{r}\delta(r - r_{ij}) + B_{ij}\frac{r}{r_{ij}^3}[1 - \Theta(r - r_{ij})]\right\}, \quad (5)$$

where $\Theta(x)$ is the Heaviside step function. Intermediate steps are carried out in Appendix *A* and accompanying supplementary materials online.[1]

Equation (5) is the basic mPDF quantity of interest. Similar to the atomic PDF for an elemental system (Farrow & Billinge, 2009) $f_{\mathrm{atPDF}}(r) = (1/rN)\sum_{i\neq j}\delta(r - r_{ij})$, the mPDF involves delta functions at spin-pair separation distances, but is

[1] Supplementary material for this article is available from the IUCr electronic archive (Reference: MQ5020).

modulated by the orientational term A_{ij}, which is positive for ferromagnetic-like correlations along the local y direction and negative for antiferromagnetic-like correlations. Moreover, the mPDF contains an additional term linear in r that is entirely absent from the atomic PDF. These complications arise from the fact that magnetic neutron scattering depends on both the spatial and orientational correlations of magnetic moments.

To get a sense of the meaning of this quantity, we integrate $rf(r)$ over an annulus with inner and outer radii a and b, respectively:

$$\int_a^b \mathrm{d}r\, rf(r) = N_{ab}\langle\cos\theta\rangle_{ab} + \frac{1}{N}\frac{1}{2S(S+1)} \times \left(\sum_{i,j\in\mathscr{S}'} B_{ij}\frac{b^3-a^3}{r_{ij}^3} - \sum_{i,j\in\mathscr{S}} B_{ij}\frac{a^3}{r_{ij}^3}\right), \qquad (6)$$

where N_{ab} is the number of spins in the annulus, the quantity $\langle\cos\theta\rangle_{ab} = (1/N)\sum_i(1/N_{ab})\sum_{j\in\mathscr{S}}\langle\cos\theta_{ij}\rangle$ is the cosine of the angle between spin i at the origin and spin j in the annulus averaged first over all spins in the annulus and then over all spins taken at the origin, $\mathscr{S}$ is the set of all spin pairs such that $a \le r_{ij} \le b$, and $\mathscr{S}'$ is the set of all pairs with $r_{ij} > b$. From this result, it is evident that the quantity $rf(r)$ is analogous to the radial distribution function $R(r)$ in the atomic PDF, but modified by additional orientational terms. Interestingly, the second term in the above result vanishes if the sum of all B_{ij} in any given shell of spins at the same radial distance from the origin is zero (as is the case for cubic symmetry, for instance) or in the limit $r_{ij} \to \infty$.

Two challenges distinguish mPDF from atomic PDF analysis. First, the magnetic form factor restricts magnetic scattering to momentum transfers of less than approximately 8–10 Å^{-1} even in the most favorable circumstances. This limits the maximum achievable real-space resolution significantly more than in the case of atomic PDF, where the form factor is less problematic for X-ray scattering and entirely absent for nuclear neutron scattering. This limitation is partially mitigated by the fact that an understanding of magnetic structure typically requires less real-space resolution than does atomic structure, since there are generally only very few magnetic moments per unit cell. Second, the somewhat more complicated analytical form of the mPDF may appear to make it rather less useful than the atomic PDF. Despite these difficulties, mPDF analysis still has the potential to offer important new insights into a variety of magnetic systems. The second difficulty mentioned can easily be remedied by examining the calculated mPDF for various systems as an intuition-building exercise. In many cases, the mPDF simplifies considerably, and in all cases it is rich with information. To illustrate this, we now present the simulated mPDF from several simple spin configurations.

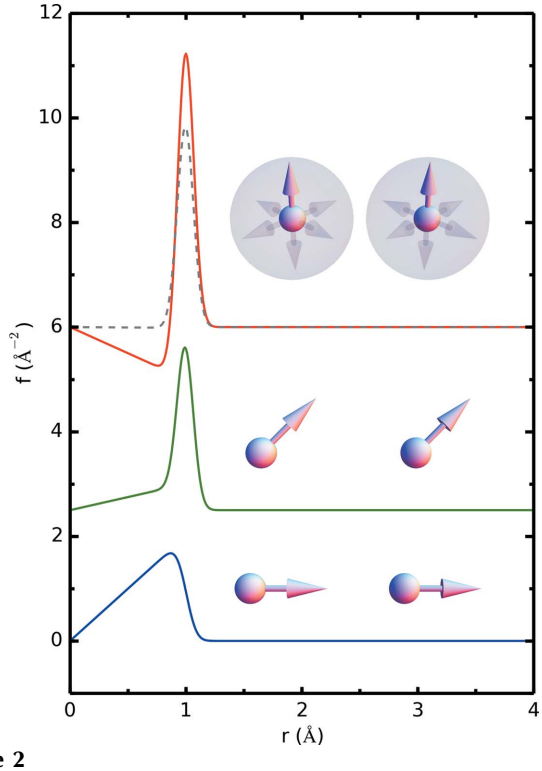

Figure 2
Calculated mPDFs from a ferromagnetically coupled pair of spins in three different orientations, showing the sensitivity of the mPDF to the exact spin orientation up to rotational invariance about the axis joining the pair. The broken line in the top portion of the figure shows the result when the average over all possible ferromagnetic orientations is calculated.

3. Simulated mPDFs from simple systems

3.1. Single pair of spins

We first consider a single pair of ferromagnetically coupled spins. The mPDF consists of a peak at the pair separation distance and a linear baseline whose slope depends on the spin orientation (Fig. 2). The positive sign of the peak indicates the ferromagnetic alignment of the spins. To represent the effect of thermal fluctuations, the sharp features of the delta and Heaviside functions have been smoothed with Gaussian and Fermi–Dirac functions, respectively. As seen in Fig. 2, the baseline and peak height depend on the orientation of the spins relative to the axis joining them, with rotational symmetry about the axis being preserved. The peak height depends on the components aligned perpendicular to the connecting axis, causing the peak to vanish altogether when the spins are aligned along the axis. In this simple case, therefore, the mPDF is sensitive to the exact orientation of the spins up to the axial rotational invariance. However, it will be seen that this sensitivity is somewhat diminished with higher symmetry and dimensionality. As an illustration of this, averaging the mPDF from the ferromagnetic pair over all possible orientations causes the baseline to vanish and reduces the peak height to 2/3 the maximal value (broken line in Fig. 2). Incidentally, this mPDF is what one would expect from a collection of uncorrelated ferromagnetic dimers. For reference, we also display the analogous results for antiferromagnetic spin pairs in Fig. 3.

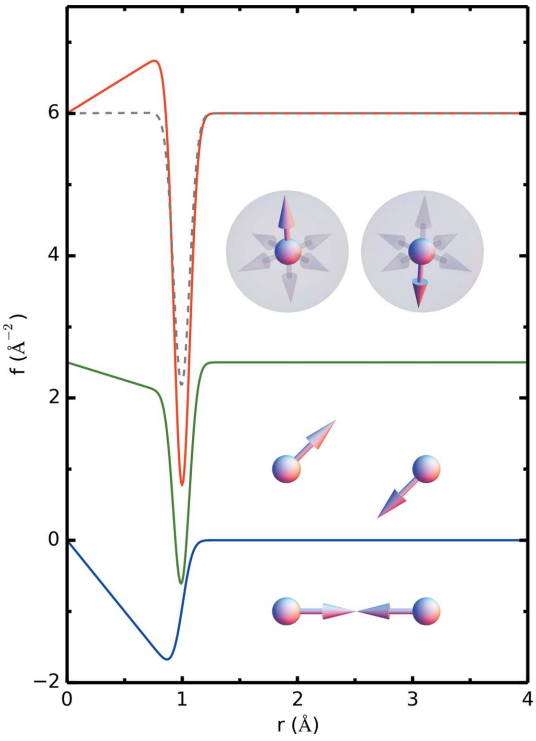

Figure 3
Calculated mPDFs from an antiferromagnetically coupled pair of spins, analogous to the ferromagnetic results presented in Fig. 2.

3.2. One-dimensional antiferromagnetic chain

The mPDF from a one-dimensional antiferromagnetic chain looks similar to the previous example, but with additional peaks appearing at integral multiples of the pair separation distance (Fig. 4). Moreover, the first peak is negative due to the antiferromagnetic coupling of nearest neighbors, while the second-nearest neighbor is positive and so on. The peak heights diminish as $1/r$ and the successive baseline slopes diminish as $1/r^3$. As before, the mPDF is sensitive to the spin orientation relative to the chain axis, but is invariant under rotations about this axis. When averaged over all possible moment directions, the baseline again vanishes (broken line in Fig. 4).

3.3. One-dimensional spin-density wave

A one-dimensional spin-density wave illustrates the intuitiveness of the mPDF. Aside from the $1/r$ envelope, the mPDF assumes precisely the same form as the actual arrangement of spins in real space (Fig. 5). The mPDF therefore provides at a glance detailed information about the spin configuration of the system. It is important to note that the changing peak height in this example is not due to changes in the spin orientations relative to the axis as in the previous examples, rather it is due to the spatially modulating magnitude of the magnetic moments. These two effects on the peak height can be distinguished from each other by examining the behavior of the baseline, although the distinctions are less apparent after orientational averaging.

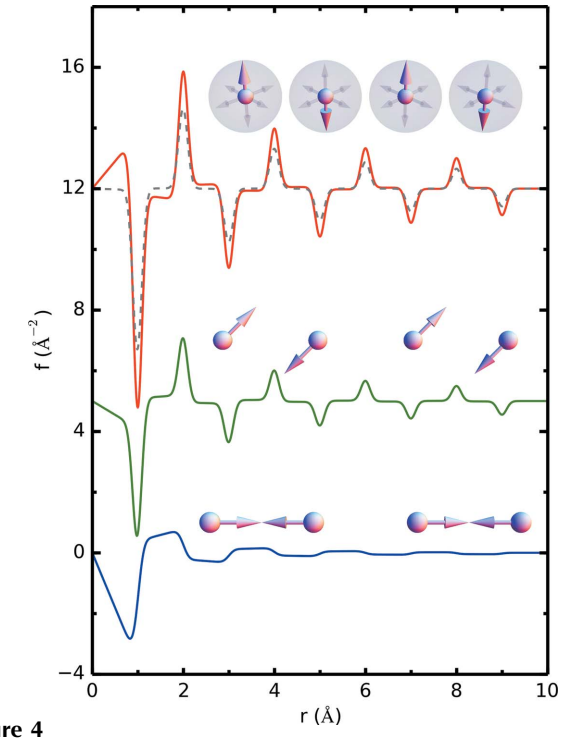

Figure 4
Calculated mPDFs from an antiferromagnetically coupled one-dimensional chain of spins in various orientations. The mPDF remains sensitive to the exact spin orientation relative to the chain axis except in the fully orientationally averaged case (broken gray line).

3.4. Simple ferromagnet and antiferromagnet

We now consider the mPDF of a cubic ferromagnet and antiferromagnet (Fig. 6). Cubic symmetry renders the mPDF insensitive to the absolute orientation of the magnetic axis and also causes the term linear in r to vanish, so that the mPDF consists only of peaks on a flat baseline. The relative peak heights reflect the coordination numbers of pairs at various

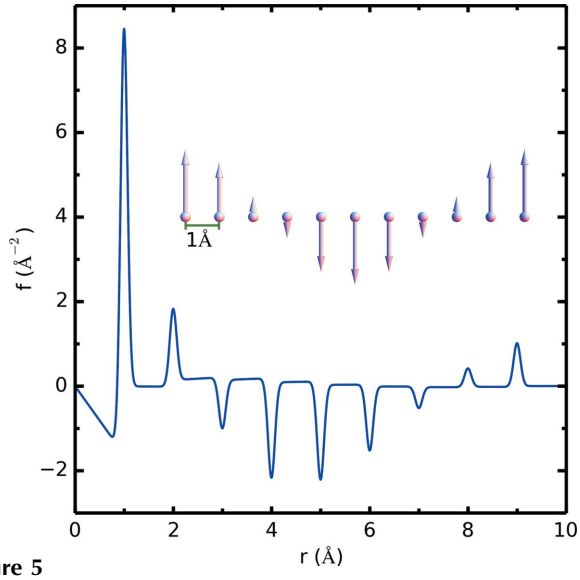

Figure 5
Calculated mPDF from a one-dimensional transverse spin-density wave, which has the exact same form as the actual real-space spin configuration, aside from the $1/r$ decay.

distances. When $rf(r)$ is plotted (broken line at the bottom of Fig. 6), the second peak has twice the height of the first, since there are 12 second-nearest neighbors and only six nearest neighbors. Corresponding height ratios are seen in the third peak (eight third-nearest neighbors), the fourth peak (six fourth-nearest neighbors) and so on. However, at large r, the coordination-shell spacings become closer together, causing the peaks to overlap. This results in a background contribution to the mPDF that increases with r at a rate determined by the average spin density of the material, albeit partially counteracted by the $1/r$ envelope. The atomic PDF has an identical average background term (Egami & Billinge, 2013; Farrow & Billinge, 2009).

3.5. Spin ice

As a final example, we consider a 'spin-ice' material frozen in one of its degenerate ground states. These systems consist of a network of corner-sharing tetrahedra with a large spin residing on each tetrahedral vertex (Balents, 2010). A strong single-ion anisotropy forces the spins to act as Ising doublets pointing either toward or away from the center of their respective tetrahedra, resulting in severe geometrical frustration of the ferromagnetically coupled spins. This leads to a macroscopically degenerate ground-state configuration defined by the so-called 'ice rules' consisting of two spins pointing in and two out on any given tetrahedron, named for the similarity to the structure of water ice (Harris *et al.*, 1997; Bramwell & Gingras, 2001).

The nontrivial spin configuration generated by the ice rules invites a more detailed analysis of the mPDF for this system (Fig. 7). A cubic lattice parameter of 10 Å has been selected for this example. The first peak, which arises from the six nearest neighbors (NN, red in Fig. 7) lying on the vertices of the two tetrahedra to which each spin belongs, is well defined and strongly negative. This can be intuitively understood in the following way. An arbitrary spin taken to be at the origin (blue in Fig. 7) will be oriented into one of its tetrahedra (the 'in-tet') and out of the other (the 'out-tet'). Of the three other spins on the in-tet, exactly one will be pointing inward; likewise, exactly one spin will be directed away from the out-tet. We will call these two spins the 'partners' of the spin at the origin. Thus, the central spin always has two partners and four 'anti-partners'. Recalling the local coordinate system introduced in equation (1), one can easily verify that, along the y direction, the partners are aligned and the anti-partners are anti-aligned with the central spin. Since peak height in the mPDF is determined by the y components of the spin pairs [the A_{ij} term in equation (5)], the four anti-partners outweigh the two partners and give rise to the negative NN peak. The mPDF immediately reveals that the ice rules combined with the geometry yield a net anti-ferromagnetic-like NN correlation in the locally defined y direction, despite the ferromagnetic NN interaction. Normally, ferromagnetically coupled spins would not be frustrated on a triangular or tetrahedral

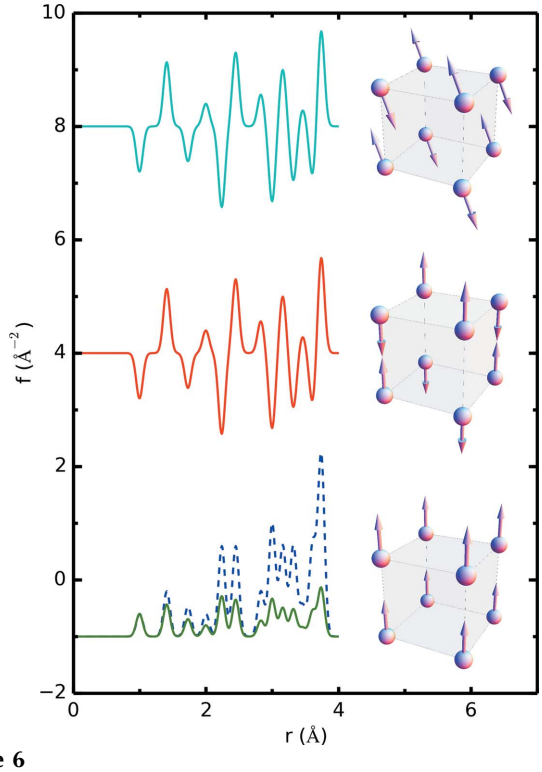

Figure 6
Calculated mPDFs from a cubic structure with various antiferromagnetic (top, middle) and ferromagnetic (bottom) spin configurations, showing the rotational invariance of the mPDF resulting from cubic symmetry. The bottom plot also displays the radial distribution function $R(r)$ with the broken line, illustrating the proportionality of peak height to coordination number as described in the body of the text.

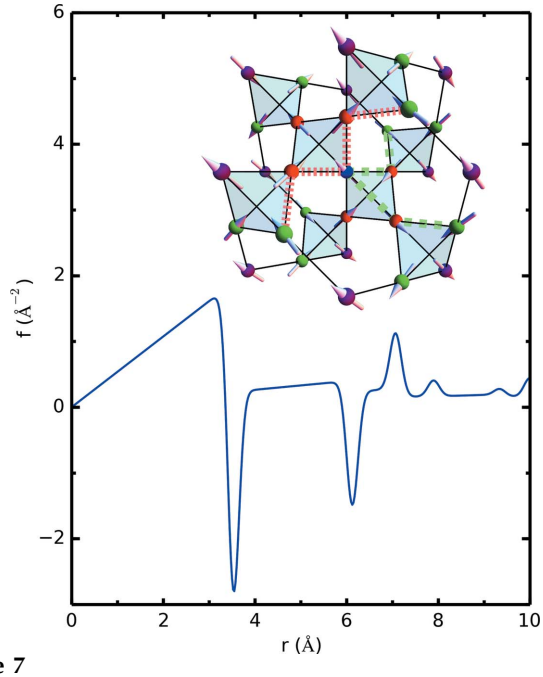

Figure 7
Calculated mPDF of the spin-ice ground-state configuration obeying the 'two-in two-out' ice rules. The inset shows one possible ground state, with one spin arbitrarily taken to be at the origin (blue), and the first-, second- and third-nearest neighbors shown in red, green and purple, respectively. The red (green) lines with short (long) dashes show the O-P-A and O-A-P (O-P-P and O-A-A) chains described in the body of the text.

lattice, but the single-ion anisotropy in this system causes frustration on the pyrochlore network.

The second peak in the mPDF corresponds to the 12 next-nearest neighbors (NNNs, green in Fig. 7), two on each of the tetrahedra adjoining the in- and out-tets of the central spin. The NNN distance is nearly double the NN distance and the coordination number is also doubled. As such, one might expect the $1/r$ decay to be offset by the increase in coordination number, resulting in a second peak of approximately the same magnitude as the first. This is clearly not the case; the NNN peak is significantly smaller in magnitude, indicative of decreased spin correlation at larger r. To understand the negative sign of the peak, we consider all possible NNN configurations. Each NN can be either a partner (P) or an anti-partner (A) of the central spin, and each NNN can in turn be either a partner or anti-partner of the NN. Therefore, the three-atom chains from the central spin (O) to the NNNs can be of the form O-P-P, O-P-A, O-A-P or O-A-A. It is not difficult to see that the O-A-P and O-P-A configurations result in positive correlations between the central spin and the NNN (red lines with short dashes in Fig. 7), whereas the O-A-A and O-P-P chains result in negative correlations (green lines with long dashes in Fig. 7), all of equal magnitude. If we make the simplifying assumption that the NNNs on different tetrahedra are independent, then elementary counting arguments show that 5/9 of the possible two-atom chains are O-A-A or O-P-P and 4/9 are O-A-P or O-P-A, thus slightly favoring the negative correlation.

Peak magnitude continues to decrease rapidly with the third and fourth peaks despite 12-fold coordination also found for the third- (purple in Fig. 7) and fourth-nearest neighbors, further illustrating the decrease in spin correlation. Both of these peaks are positive, since the ice rules allow a slightly greater number of configurations with aligned y components than anti-aligned. Peaks at higher r are similarly damped while oscillating between positive and negative until the mPDF is essentially zero for r greater than several lattice parameters. Despite the inherent randomness in this system resulting from the frustration, the mPDF shows that correlations nonetheless exist out to relatively high r due to the combinatorics of the finite number of different paths to far neighbors from the central spin. In this way, we see that the mPDF gives direct access to details of the spin configuration and the finite correlation length in the spin-ice ground state.

4. Orbital contributions and multiple magnetic species

The expression for the mPDF derived previously applies to systems in which the magnetism arises solely from localized spins of a single type of magnetic ion. Many systems of interest, including spin liquids and spin ices, fall into this category, but it is also useful to extend our results to systems with multiple magnetic species and both spin and orbital angular momentum contributions.

In the dipole approximation, *i.e.* when the mean radius of the wavefunction of the unpaired electrons is much less than κ^{-1}, the contributions from orbital angular momentum can be included by replacing the magnetic form factor $f(\kappa)$ with $\frac{1}{2}gf(\kappa)$, where the Landé g factor is (Lovesey, 1984; Squires, 1996)

$$g = g_S + g_L = \frac{J(J+1) - L(L+1) + S(S+1)}{J(J+1)} + \frac{J(J+1) + L(L+1) - S(S+1)}{2J(J+1)} \quad (7)$$

$$= 1 + \frac{J(J+1) - L(L+1) + S(S+1)}{2J(J+1)} \quad (8)$$

and the full form factor is

$$f(\kappa) = \mathscr{J}_0 \frac{g_S}{g} + (\mathscr{J}_0 + \mathscr{J}_2)\frac{g_L}{g}, \quad (9)$$

with

$$\mathscr{J}_n = 4\pi \int_0^\infty \mathrm{d}r\, r^2 j_n(\kappa r)|\Phi(r)|^2, \quad (10)$$

j_n being a spherical Bessel function of order n and $\Phi(r)$ the radial wavefunction of the electrons. Allowing for different values of these quantities for α different magnetic species, the orientationally averaged differential scattering cross section becomes

$$\frac{\mathrm{d}\sigma}{\mathrm{d}\Omega} = \frac{2}{3}(\gamma r_0)^2 \sum_\alpha N_\alpha \left(\frac{1}{2} g_\alpha f_\alpha\right)^2 J_\alpha(J_\alpha + 1) + (\gamma r_0)^2 \sum_{i \neq j} \left(\frac{1}{2} g_i f_i\right)\left(\frac{1}{2} g_j f_j\right) \times \left\{ A_{ij} \frac{\sin \kappa r_{ij}}{\kappa r_{ij}} + B_{ij}\left[\frac{\sin \kappa r_{ij}}{(\kappa r_{ij})^3} - \frac{\cos \kappa r_{ij}}{(\kappa r_{ij})^2}\right]\right\}. \quad (11)$$

For notational compactness, we define a quantity $\ell \equiv (\gamma r_0/2) g f(\kappa)[(2/3)J(J+1)]^{1/2}$. We also employ the Morningstar–Warren approximation, in which the magnetic form factors for each magnetic species are replaced by an average magnetic form factor $\overline{f(\kappa)} = (1/N_\alpha)\sum_\alpha c_\alpha f_\alpha(\kappa)$, where c_α is the fractional proportion of the αth spin. In the X-ray scattering version of the Morningstar–Warren approximation, it is necessary to first rewrite the form factor as $f(\kappa) = f(0)\tilde{f}(\kappa)$, where $f(0)$ is approximately equal to the atomic number of the scattering atom and $\tilde{f}(\kappa)$ contains the κ dependence of the form factor, with a value of 1 at $\kappa = 0$. This is not necessary for magnetic neutron scattering, since it is evident from the definitions above that $f(0) = 1$. In practice, empirically measured magnetic form factors tabulated in *International Tables of Crystallography* Volume C (Wilson, 1995) or other resources can be used and appropriately weighted to obtain the average magnetic form factor. With these simplifications, the scattering cross section can be expressed as

$$\frac{\mathrm{d}\sigma}{\mathrm{d}\Omega} = N\langle \ell^2 \rangle + \left(\frac{\gamma r_0}{2}\right)^2 \overline{f(\kappa)}^2 \sum_{i \neq j} g_i g_j \times \left\{ A_{ij} \frac{\sin \kappa r_{ij}}{\kappa r_{ij}} + B_{ij}\left[\frac{\sin \kappa r_{ij}}{(\kappa r_{ij})^3} - \frac{\cos \kappa r_{ij}}{(\kappa r_{ij})^2}\right]\right\}, \quad (12)$$

where

$$\langle \ell^2 \rangle = \frac{2}{3}\left(\frac{\gamma r_0}{2}\right)^2 \overline{f(\kappa)}^2 \sum_\alpha c_\alpha g_\alpha^2 J_\alpha (J_\alpha + 1).$$

As in the atomic PDF, we define the total structure factor through

$$S(\kappa) - 1 = \frac{\mathrm{d}\sigma/\mathrm{d}\Omega}{N\langle \ell \rangle^2} - \frac{\langle \ell^2 \rangle}{\langle \ell \rangle^2}. \quad (13)$$

Substituting in our expression for the scattering cross section, this becomes

$$S(\kappa) - 1 = \frac{1}{N}\frac{3}{2\langle g[J(J+1)]^{1/2}\rangle^2}\sum_{i\neq j} g_i g_j \times \left\{ A_{ij}\frac{\sin \kappa r_{ij}}{\kappa r_{ij}} + B_{ij}\left[\frac{\sin \kappa r_{ij}}{(\kappa r_{ij})^3} - \frac{\cos \kappa r_{ij}}{(\kappa r_{ij})^2}\right]\right\}, \quad (14)$$

where

$$\langle g[J(J+1)]^{1/2}\rangle = \sum_\alpha c_\alpha g_\alpha [J_\alpha (J_\alpha + 1)]^{1/2}.$$

The reduced structure function and the Fourier transform are

$$F(\kappa) = \frac{1}{N}\frac{3}{2\langle g[J(J+1)]^{1/2}\rangle^2}\sum_{i\neq j} g_i g_j \times \left[A_{ij}\frac{\sin \kappa r_{ij}}{r_{ij}} + B_{ij}\left(\frac{\sin \kappa r_{ij}}{\kappa^2 r_{ij}^3} - \frac{\cos \kappa r_{ij}}{\kappa r_{ij}^2}\right)\right] \quad (15)$$

and

$$f(r) = \frac{1}{N}\frac{3}{2\langle g[J(J+1)]^{1/2}\rangle^2}\sum_{i\neq j} g_i g_j \times \left\{ \frac{A_{ij}}{r}\delta(r - r_{ij}) + B_{ij}\frac{r}{r_{ij}^3}[1 - \Theta(r - r_{ij})]\right\}, \quad (16)$$

respectively. The effect of multiple magnetic species with orbital contributions is therefore to weight the contribution of each pair by the Landé splitting factors. Interestingly, this result reduces to equation (5) in the case of spin-only scattering even for multiple spin species, as long as the replacement

$$S(S+1) \rightarrow \langle [S(S+1)]^{1/2}\rangle^2 = \{\sum_\alpha c_\alpha [S_\alpha (S_\alpha + 1)]^{1/2}\}^2$$

is made. This simplification arises from the fact that g is always 2 for spins, regardless of the value of the spin quantum number S.

5. Measurements with polarized neutrons

The mPDF technique relies on the ability to accurately obtain the magnetic neutron scattering cross section. This can present a significant experimental challenge if unpolarized neutrons are used, since it is a nontrivial task to separate the magnetic from the nuclear scattering. For this reason, it can be highly advantageous to use a polarized incident neutron beam and analyze the polarization of the scattered neutrons, allowing the unambiguous separation of magnetic, nuclear and spin-incoherent cross sections by taking linear combinations of the different scattering channels, *i.e.* spin-flip and non-spin-flip, for various configurations of the incident polarization direction and the scattering vector (Lovesey, 1984; Squires, 1996). Such linear combinations must be carefully chosen so as to remove nuclear-magnetic interference terms, leaving only the magnetic contribution. Once the full magnetic scattering signal has been isolated, the mPDF equations derived previously may be applied without any modification, even though equation (1) is based on the assumption of an unpolarized neutron beam. The cross section for unpolarized neutrons is simply the sum of the spin-flip and non-spin-flip scattering channels, so the full magnetic scattering obtained from polarization analysis is precisely what would be obtained from unpolarized neutrons if the magnetic scattering could be unambiguously separated from the nuclear scattering.

Several experimental methods have been devised to obtain information from polarized neutron scattering, ranging in complexity from the simple uniaxial parallel–perpendicular method to the highly sophisticated techniques of full vector polarization analysis (Roessli & Böni, 2002). The advantages of vector polarization analysis are generally lost on powder samples, so it may be more suitable to use the simpler longitudinal polarization analysis techniques for the purposes of mPDF. A particularly attractive choice is *XYZ* polarization analysis (Schärpf & Capellmann, 1993), which produces the correct linear combinations to recover the full magnetic scattering signal and utilizes a large bank of detectors covering a wide solid angle to make data collection more efficient (Stewart *et al.*, 2000, 2009; Schweika, 2010).

6. Summary

We have introduced mPDF analysis as a novel approach for investigating short-range magnetic correlations, by Fourier transforming the total magnetic scattering intensity into real space. The mPDF equations derived in this paper form the starting point for quantitative fitting of magnetic structural models to experimentally obtained mPDF signals. Through several examples from simple systems, we have shown the intuitive nature of the mPDF, which will be highly useful in understanding and modeling local magnetic structure. As with atomic PDF analysis, we expect this method to have the largest impact on systems exhibiting magnetic short-range order, nanomagnets, molecular magnets and so on.

APPENDIX *A*
Derivation of the mPDF equations

In this Appendix, we provide the intermediate steps involved in several of the equations in the preceding derivation of the mPDF equations. Going from equations (4) to (5), we have

$$f(r) = \frac{2}{\pi}\int_0^\infty \mathrm{d}\kappa\, F(\kappa)\sin\kappa r \tag{17}$$

$$= \frac{2}{\pi}\frac{1}{N}\frac{3}{2S(S+1)}\sum_{i\neq j}\frac{1}{r_{ij}}\left(A_{ij}\int_0^\infty \mathrm{d}\kappa \sin\kappa r\sin\kappa r_{ij} + \frac{B_{ij}}{r_{ij}^2}\int_0^\infty \mathrm{d}\kappa \frac{\sin\kappa r\sin\kappa r_{ij}}{\kappa^2} - \frac{B_{ij}}{r_{ij}}\int_0^\infty \mathrm{d}\kappa \frac{\sin\kappa r\cos\kappa r_{ij}}{\kappa}\right) \tag{18}$$

$$= \frac{2}{\pi}\frac{1}{N}\frac{3}{2S(S+1)}\sum_{i\neq j}\frac{1}{r_{ij}}\left[A_{ij}\frac{\pi}{2}\delta(r-r_{ij}) + \frac{B_{ij}}{r_{ij}^2}\frac{\pi}{4}(r+r_{ij}-|r-r_{ij}|) - \frac{B_{ij}}{r_{ij}}\frac{\pi}{4}2\Theta(r-r_{ij})\right] \tag{19}$$

$$= \frac{1}{N}\frac{3}{2S(S+1)}\sum_{i\neq j}\frac{1}{r_{ij}}\left[A_{ij}\delta(r-r_{ij}) + \frac{1}{2}\frac{B_{ij}}{r_{ij}^2}(r+r_{ij}-|r-r_{ij}|) - \frac{B_{ij}}{r_{ij}}\Theta(r-r_{ij})\right]. \tag{20}$$

The integrals in the second equality are straightforward but nontrivial, and are worked out explicitly in the online supplementary material. For a single pair of spins,

$$f_{ij}(r<r_{ij}) = \frac{1}{N}\frac{3}{2S(S+1)}B_{ij}\frac{r}{r_{ij}^3}, \tag{21}$$

$$f_{ij}(r=r_{ij}) = \frac{1}{N}\frac{3}{2S(S+1)}\left[\frac{A_{ij}}{r}\delta(r-r_{ij}) + \frac{B_{ij}}{2r^2}\right] \tag{22}$$

and

$$f_{ij}(r>r_{ij}) = 0. \tag{23}$$

This function is therefore more concisely written as

$$f(r) = \frac{1}{N}\frac{3}{2S(S+1)}\sum_{i\neq j}\left\{\frac{A_{ij}}{r}\delta(r-r_{ij}) + B_{ij}\frac{r}{r_{ij}^3}[1-\Theta(r-r_{ij})]\right\}, \tag{24}$$

which is equation (5). Here we have utilized the convention for the Heaviside step function that $\Theta(0) = \frac{1}{2}$.

We now calculate the integral in equation (6):

$$\int_a^b \mathrm{d}r\, rf(r) = \frac{1}{N}\frac{3}{2S(S+1)} \times \sum_{i\neq j}\int_a^b \mathrm{d}r\left\{A_{ij}\delta(r-r_{ij}) + B_{ij}\frac{r^2}{r_{ij}^3}[1-\Theta(r-r_{ij})]\right\} \tag{25}$$

$$= \frac{1}{N}\frac{3}{2S(S+1)}\sum_{i,j\in\mathscr{S}}A_{ij} + \frac{1}{N}\frac{3}{2S(S+1)} \times \sum_{i\neq j}\frac{B_{ij}}{r_{ij}^3}\begin{cases}0 & \text{if } r_{ij}<a\\ \frac{1}{3}(r_{ij}^3-a^3) & \text{if } a\le r_{ij}\le b\\ \frac{1}{3}(b^3-a^3) & \text{if } r_{ij}>b\end{cases} \tag{26}$$

$$= \frac{1}{N}\frac{3}{2S(S+1)}\left\{\sum_{i,j\in\mathscr{S}}\left[A_{ij}+\frac{1}{3}B_{ij}\left(\frac{r_{ij}^3-a^3}{r_{ij}^3}\right)\right] + \frac{1}{3}\sum_{i,j\in\mathscr{S}'}B_{ij}\left(\frac{b^3-a^3}{r_{ij}^3}\right)\right\} \tag{27}$$

$$= \frac{1}{N}\frac{3}{2S(S+1)}\left\{\sum_{i,j\in\mathscr{S}}\left[\frac{2}{3}\langle S_i^xS_j^x + S_i^yS_j^y\rangle - \frac{1}{3}B_{ij}\left(\frac{a}{r_{ij}}\right)^3\right] + \frac{1}{3}\sum_{i,j\in\mathscr{S}'}B_{ij}\left(\frac{b^3-a^3}{r_{ij}^3}\right)\right\} \tag{28}$$

$$= \frac{1}{N}\sum_{i,j\in\mathscr{S}}\left[\frac{\langle\mathbf{S}_i\cdot\mathbf{S}_j\rangle}{S(S+1)} - \frac{1}{2S(S+1)}B_{ij}\frac{a^3}{r_{ij}^3}\right] + \frac{1}{N}\frac{1}{2S(S+1)}\sum_{i,j\in\mathscr{S}'}B_{ij}\frac{b^3-a^3}{r_{ij}^3} \tag{29}$$

$$= N_{ab}\langle\cos\theta\rangle_{ab} + \frac{1}{N}\frac{1}{2S(S+1)} \times \left(\sum_{i,j\in\mathscr{S}'}B_{ij}\frac{b^3-a^3}{r_{ij}^3} - \sum_{i,j\in\mathscr{S}}B_{ij}\frac{a^3}{r_{ij}^3}\right). \tag{30}$$

We have used the result that for identical spins, $\mathbf{S}_i\cdot\mathbf{S}_j = \hat{S}^2\cos\theta_{ij}$, and the operator $\hat{S}^2$ has the eigenvalue $S(S+1)$. We have also recalled the fact that the local coordinate system being utilized is defined such that $S_i^z = 0$, which allows the introduction of the dot product $\mathbf{S}_i\cdot\mathbf{S}_j$ in the fifth equality.

This work was supported by the US National Science Foundation Partnership in International Research and Education initiative (PIRE) *via* grant No. PIRE: OISE-0968226 and the US Department of Energy, Office of Basic Energy Sciences, under contract No. DE-AC02-98CH10886.

References

Balents, L. (2010). *Nature (London)*, **464**, 199–208.
Basov, D. N. & Chubukov, A. V. (2011). *Nat. Phys.* **7**, 272–276.
Billinge, S. J. L. & Kanatzidis, M. G. (2004). *Chem. Commun.* **2004**, 749–760.
Billinge, S. J. L. & Levin, I. (2007). *Science*, **316**, 561–565.
Blech, I. A. & Averbach, B. L. (1964). *Physics*, **1**, 31–44.
Bokov, A. A. & Ye, Z.-G. (2006). *J. Mater. Sci.* **41**, 31–52.
Bramwell, S. T. & Gingras, M. J. P. (2001). *Science*, **294**, 1495–1501.
Cheong, S.-W. & Mostovoy, M. (2007). *Nat. Mater.* **6**, 13–20.
Chuang, Y., Gromko, A., Dessau, D., Kimura, T. & Tokura, Y. (2001). *Science*, **292**, 1509–1513.
Cross, L. E. (1987). *Ferroelectrics*, **76**, 241–267.
Dagotto, E. (1994). *Rev. Mod. Phys.* **66**, 763–840.
Dagotto, E. (2005). *Science*, **309**, 257–262.
Dagotto, E., Burgy, J. & Moreo, A. (2003). *Solid State Commun.* **126**, 9–22.
Dagotto, E., Hotta, T. & Moreo, A. (2001). *Phys. Rep.* **344**, 1–153.
Eerenstein, W., Mathur, N. D. & Scott, J. F. (2006). *Nature (London)*, **442**, 759–765.
Egami, T. & Billinge, S. J. L. (2013). *Underneath the Bragg Peaks: Structural Analysis of Complex Materials*, 2nd ed. Amsterdam: Elsevier.
Farrow, C. L. & Billinge, S. J. L. (2009). *Acta Cryst.* A**65**, 232–239.

Fath, M., Freisem, S., Menovsky, A. A., Tomioka, Y., Aarts, J. & Mydosh, J. A. (1999). *Science*, **285**, 1540–1542.
Furdyna, J. K. (1988). *J. Appl. Phys.* **64**, R29–R64.
Han, T.-H., Helton, J. S., Chu, S., Nocera, D. G., Rodriguez-Rivera, J. A., Broholm, C. & Lee, Y. S. (2012). *Nature (London)*, **492**, 406–410.
Harris, M. J., Bramwell, S. T., McMorrow, D. F., Zeiske, T. & Godfrey, K. W. (1997). *Phys. Rev. Lett.* **79**, 2554–2557.
Imada, M., Fujimori, A. & Tokura, Y. (1998). *Rev. Mod. Phys.* **70**, 1039–1263.
Juhás, P., Cherba, D. M., Duxbury, P. M., Punch, W. F. & Billinge, S. J. L. (2006). *Nature (London)*, **440**, 655–658.
Keen, D. A. & McGreevy, R. L. (1991). *J. Phys. Condens. Matter*, **3**, 7383–7394.
Lee, P. A., Nagaosa, N. & Wen, X.-G. (2006). *Rev. Mod. Phys.* **78**, 17–85.
Lovesey, S. W. (1984). *Theory of Neutron Scattering from Condensed Matter*, Vol. 2. Oxford: Clarendon Press.
Millis, A. J. (1998). *Nature (London)*, **392**, 147–150.
Ohno, H. (1998). *Science*, **281**, 951–956.
Orenstein, J. & Millis, A. J. (2000). *Science*, **288**, 468–474.
Paddison, J. A. M. & Goodwin, A. L. (2012). *Phys. Rev. Lett.* **108**, 017204.
Proffen, T., Billinge, S. J. L., Egami, T. & Louca, D. (2003). *Z. Kristallogr.* **218**, 132–143.
Roessli, B. & Böni, P. (2002). *Polarized Neutron Scattering*, ch. 2.8.5 in *Scattering: Scattering and Inverse Scattering in Pure and Applied Science*, edited by R. Pike & P. Sabatier. London: Academic Press.
Schärpf, O. & Capellmann, H. (1993). *Phys. Status Solidi*, **135**, 359–379.
Schweika, W. (2010). *J. Phys. Conf. Ser.* **211**, 012026.
Squires, G. L. (1996). *Introduction to the Theory of Thermal Neutron Scattering*. New York: Dover Publications.
Stewart, J. R., Andersen, K. H., Cywinski, R. & Murani, A. P. (2000). *J. Appl. Phys.* **87**, 5425–5430.
Stewart, J. R., Deen, P. P., Andersen, K. H., Schober, H., Barthélémy, J.-F., Hillier, J. M., Murani, A. P., Hayes, T. & Lindenau, B. (2009). *J. Appl. Cryst.* **42**, 69–84.
Tranquada, J. M., Axe, J. D., Ichikawa, N., Moodenbaugh, A. R., Nakamura, Y. & Uchida, S. (1997). *Phys. Rev. Lett.* **78**, 338–341.
Tranquada, J. M., Axe, J. D., Ichikawa, N., Nakamura, Y., Uchida, S. & Nachumi, B. (1996). *Phys. Rev. B*, **54**, 7489–7499.
Tucker, M. G., Dove, M. T. & Keen, D. A. (2001). *J. Appl. Cryst.* **34**, 630–638.
Tucker, M. G., Keen, D. A., Dove, M. T., Goodwin, A. L. & Hui, Q. (2007). *J. Phys. Condens. Matter*, **19**, 335218.
Uehara, M., Mori, S., Chen, C. H. & Cheong, S.-W. (1999). *Nature (London)*, **399**, 560–563.
Wilson, A. J. C. (1995). *International Tables for Crystallography*, Vol. C. Dordrecht: Kluwer Academic Publishers.
Wu, Y., Dmowski, W. & Egami, T. (1987). *J. Appl. Phys.* **61**, 3219–3224.
Young, C. A. & Goodwin, A. L. (2011). *J. Mater. Chem.* **21**, 6464–6476.
Zhao, K. *et al.* (2013). *Nat. Commun.* **4**, 1442.